

# High temperature phase stabilized microstructure in Mg–Zn–Sn alloys with Y and Sb additions

Anton Gorny · Menahem Bamberger ·  
Alexander Katsman

Received: 13 March 2007 / Accepted: 17 July 2007 / Published online: 23 August 2007  
© Springer Science+Business Media, LLC 2007

**Abstract** Mg–Zn–Sn alloys exhibit poor structural stability at elevated temperatures that restricts utilization of these alloys. Small additions of alloying elements forming high temperature phases (HTP) were used to improve the structural stability of the Mg–Zn–Sn alloy. The main goal of this work was to investigate the microstructure evolution of the Mg–Zn–Sn-alloy with additions of Y and Sb during a wide scope of heat treatments, and to elucidate peculiarities of an HTP-stabilized microstructure. In order to clarify the substructure features and phase precipitation after each step of the heat treatment, XRD, TEM, SEM and EDS analyses were applied. It was found that in the dendrite structure formed during solidification, HTP-particles are concentrated in the interdendrite regions. Solution treatment of the as-cast structure at 440 °C for 96 h lead to the formation of  $\alpha$ -Mg grains of 50–80  $\mu\text{m}$  in diameter with a characteristic substructure. The presence of HTP-particles prevented dislocation recovery and movement of dislocation walls during solution treatment, and by this way restricted annihilation of grain boundaries between dendrites of close orientation, and lead to the formation of a substructure with sub-grains of 20–30  $\mu\text{m}$ . The sub-grain boundaries are pinned by HTP-particles and are strengthened by the  $\text{MgZn}_2$  and  $\text{Mg}_2\text{Sn}$  binary precipitates during aging. Precipitate depleted zones formed near grain- and sub-grain boundaries during aging were bordered by a “crust” of enlarged binary particles. Such pinned sub-grain microstructure provides a

high structural stability of the alloys at elevated temperatures.

## Introduction

Extensive experimental research work was devoted to the Mg–Zn–Sn system considered a promising candidate for a creep resistant Mg-alloy strengthened by precipitation hardening [1–5]. Precipitation hardening is usually considered the result of interaction between dislocations and new phase particles precipitated during aging. In the case of Mg–Zn–Sn alloys,  $\text{MgZn}_2$  and  $\text{Mg}_2\text{Sn}$  intermetallic phases distributed within the Mg grains were found to be responsible for strengthening the  $\alpha$ -Mg-matrix. However, the coarsening process leading to overaging substantially diminishes the strengthening effect within 96 hours of aging [1, 2]. Positive effects of bismuth and antimony additions on the mechanical properties of AZ91 magnesium alloy were reported [6, 7]. It was also found that small yttrium additions (0.6 wt.%) improve the structural stability of the Mg–Zn–Sn alloy [8]. The presence of high temperature ternary phase  $\text{MgSnY}$  was proposed to be the stabilizing factor. However, the mechanism of structure stabilization was not elucidated. The present work was undertaken in order to investigate the microstructure evolution of the Mg–Zn–Sn-alloy with additions of Y and Sb which form stable high temperature phases (HTP) in the Mg–Zn–Sn-system and to elucidate a mechanism of HTP-influence on the microstructure stability. In order to clarify the features of substructure and phase precipitation after each heat treatment step, X-ray diffraction (XRD), scanning electron microscopy (SEM) equipped with an energy-dispersive X-ray spectrometer

A. Gorny · M. Bamberger · A. Katsman (✉)  
Department of Materials Engineering, Technion—Israel Institute  
of Technology, Haifa 32000, Israel  
e-mail: akatsman@tx.technion.ac.il

(EDS), and transmission electron microscopy (TEM) analyses were applied.

## Experimental

Pure Magnesium of 99.98% was melted in a cemented graphite crucible under protective atmosphere of 1 L/min CO<sub>2</sub> and a 60 cc/min HFC134A gas mixture. 99.8% pure zinc and 99.95% pure Sn were added to the melt. Yttrium was added to the melt as a pre-alloy containing about 30 at.% of Y (alloy 1). Pure 99.95% Sb was added to the melt (alloy 2). The melt was poured at a temperature of 720 °C into a steel disc shaped mold of 60 mm in diameter and 9 mm thick. The mold was heated up to 300 °C. The compositions of the as-cast alloys determined by Dirats labs (USA) are given in Table 1.

Samples for solution treatment were encapsulated in a quartz tube filled with Ar at a pressure of 400 mmHg. The solution treatment includes the following steps: 96 h exposure at 300 °C, heating to 440 °C at a rate of 1 °C/h and holding at this temperature for additional 96 h, followed by water quenching.

Aging was conducted in a molten salt (sodium nitrate 50% + potassium nitrate 50%) in the temperature range of 150–225 °C for 1 h to 16 days.

The specimens were sliced at 1/3 of their height for micro-structural characterization, thereby ensuring equal solidification conditions for the examined cross-sections. The specimens were prepared for SEM + EDS, TEM and XRD structural and compositional analyses.

## Results

In order to clarify the influence of Y and Sb additions on the evolution of the alloy microstructure, it was decided to start from the structure of the as-cast alloys, study the solution treated alloys and then investigate the alloy's microstructure after different aging periods at different temperatures. The microstructure of the alloys was investigated by XRD, SEM equipped with EDS, and TEM techniques including high-resolution TEM.

**Table 1** Chemical compositions of the Mg–Sn–Zn–Y(Sb) alloys (wt.%) determined by Dirats labs (USA)

	Mg	Sn	Zn	Y	Sb
Alloy 1	Balance	4	4.4	0.6	–
Alloy 2	Balance	4.4	4.4	–	1.1

## Microstructure of the as-cast alloys

Study of the microstructure of the as-cast alloys was conducted by SEM + EDS. SEM micrographs (Fig. 1) revealed a dendrite structure and the phases located mainly in the interdendritic (gray) regions.

In alloy 1 (with Y-addition) (Figs. 1a, b), the phases were identified by XRD as MgZn/Mg eutectics and Mg<sub>2</sub>Sn. (Fig. 2a). A ternary primitive orthorhombic phase MgSnY was identified by SEM + EDS and high resolution TEM. The measurements conducted on the latter phase (10 μm-sized) allowed determining the composition ratio of Mg–Sn–Y as 1:1:1. Details of the ternary phase identification were described in [3]. The Zn and Sn content in the α-Mg matrix is lower than the average alloy composition and the α-Mg has no detectable traces of Y. The interdendritic (gray) regions are enriched with Zn and Sn up to 8 wt.% and contain a minor amount of Y. Alloy 2 (with Sb addition) has a structure similar to that of alloy 1 (Fig. 1c, d): Mg<sub>2</sub>Sn and MgZn/Mg eutectics are also located in the interdendritic regions. The binary high temperature phase Mg<sub>3</sub>Sb<sub>2</sub> was also found there (Figs. 1d, 2b). Traces of Sb were detected in the α-Mg matrix.

## Microstructure of solution treated Mg–Sn–Zn–Y (Sb) alloys

Solution treatment of the alloys was conducted in accordance with the procedure described above. It resulted in full dissolution of the MgZn and Mg<sub>2</sub>Sn phases (Fig. 3). Ternary MgSnY particles in alloy 1 and binary particles Mg<sub>3</sub>Sb<sub>2</sub> in alloy 2 were not dissolved (Fig. 4) and can be clearly seen in the micrographs.

The composition of the α-Mg-matrix was measured utilizing STEM EDS. The results are presented in Table 2. The matrix of alloy 1 is depleted of Sn, which was apparently consumed, at least partially, by the ternary MgSnY-phase.

## Microstructure of the aged Mg–Sn–Zn–Y(Sb) alloys

Solution treated specimens of the alloys were aged at different temperatures (in the range of 150–225 °C) for different times (from 1 h to 16 days). It was found that homogeneous precipitation of MgZn<sub>2</sub>-phase took place in the α-Mg matrix at early stages of aging. After 4 hours of aging at 175 °C long MgZn<sub>2</sub>-needles, with an aspect ratio l/w of up to 15 were homogeneously distributed in the body of grains (Fig. 5). Heterogeneous precipitation of short needles (l/w of about 3 ÷ 4) (Fig. 5) at sub-grain boundaries and dislocations was also recognized. All

**Fig. 1** Dendrite microstructure of the alloys in the as-cast condition: (a, b)—alloy 1; (c, d)—alloy 2; (a, c) low magnification; (b, d) high magnification

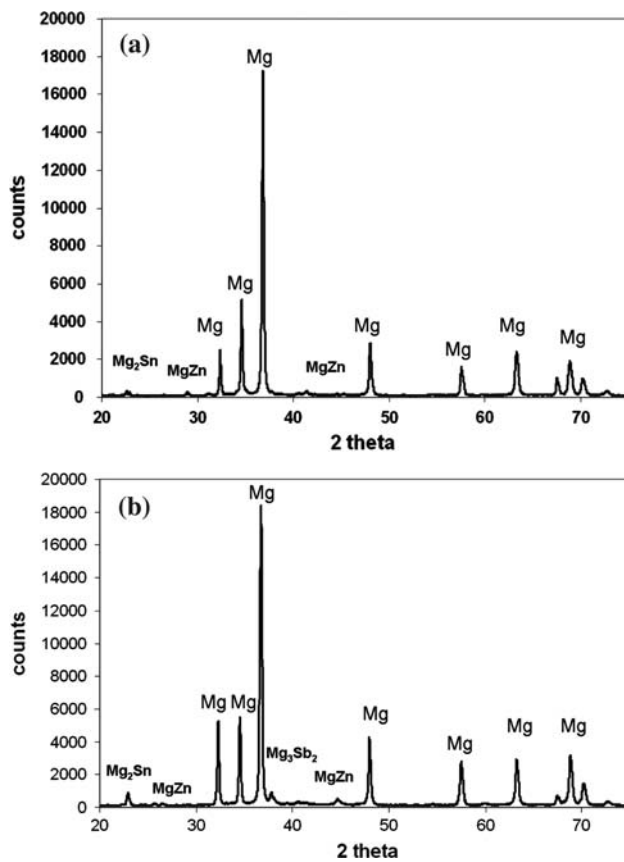
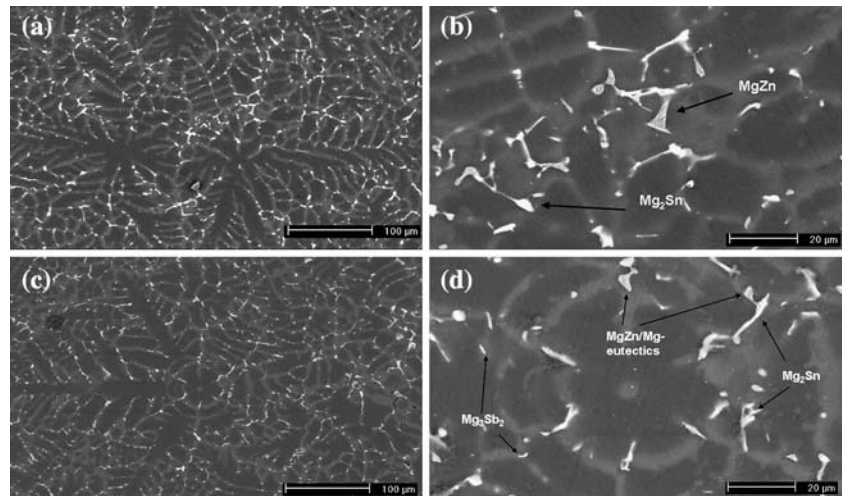


**Fig. 2** XRD spectrum of the as-cast alloys: (a) Alloy 1: MgZn and Mg<sub>2</sub>Sn were identified; (b) Alloy 2: MgZn, Mg<sub>2</sub>Sn and Mg<sub>3</sub>Sb<sub>2</sub> were identified

MgZn<sub>2</sub>-needles inside the grain were aligned in the same direction. It should be noted that the orientation of needles remains almost unchanged across the sub-grain boundaries (Fig. 5), and also the needles decorating a sub-grain boundary have the same orientation as those in the grain body. As previously found [3], the MgZn<sub>2</sub>-phase grows

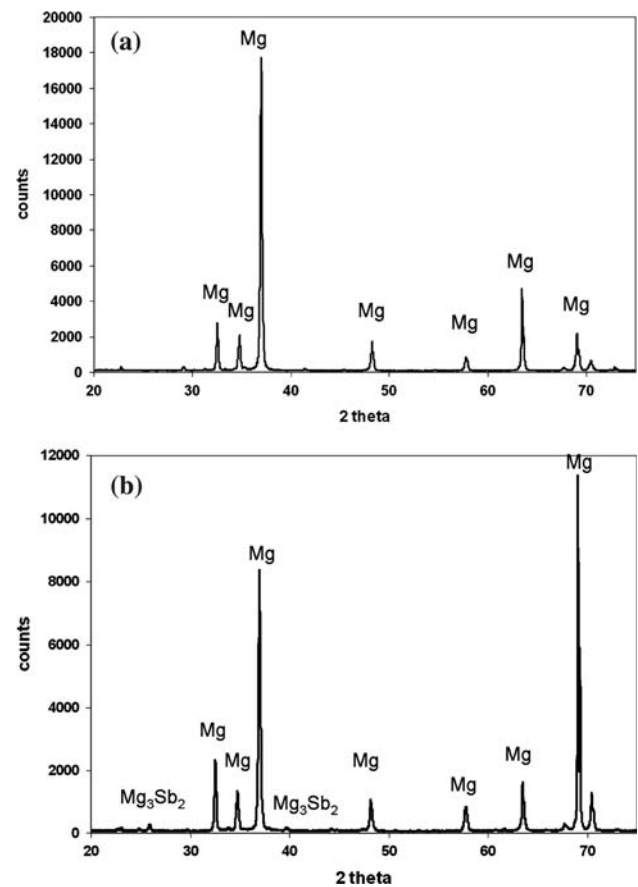


**Fig. 3** XRD spectrum of the alloys after solution treatment: (a) Alloy 1; (b) Alloy 2: an Mg<sub>3</sub>Sb<sub>2</sub> phase is identified

coherently with the  $\alpha$ -Mg with the following orientation relationship:

$$(11\bar{2}0)_{\text{MgZn}_2} \parallel \langle 1\bar{1}00 \rangle_{\text{MgZn}_2} \parallel (0002)_{\alpha\text{-Mg}} \parallel \langle 11\bar{2}0 \rangle_{\alpha\text{-Mg}} \quad (1)$$

**Fig. 4** SEM micrograph of the (a) Mg–Sn–Zn–Y and (b) Mg–Sn–Zn–Sb alloys after solution treatment

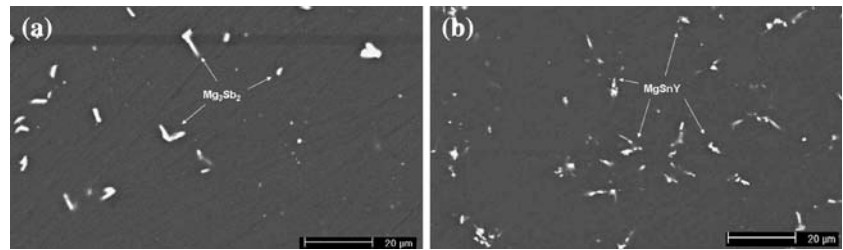


**Table 2** Compositions of the  $\alpha$ -Mg matrix (wt.%) in the solution treated alloys measured by STEM EDS

Element	Alloy 1	Alloy 2
Mg	Balance	Balance
Zn	4.4	4.4
Sn	2.2	4.2
Y	not detectable	–
Sb	–	0.2

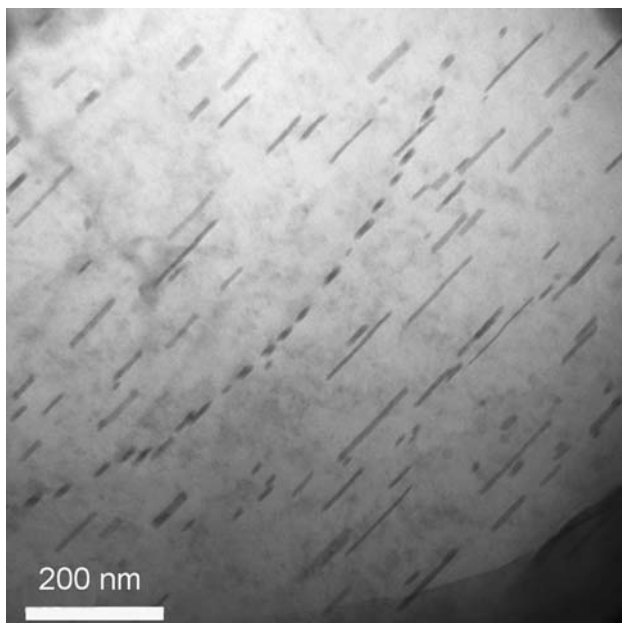


**Fig. 5** TEM micrograph of the Mg–Sn–Zn–Y alloy after aging for 4 h at 175 °C; curved sub-grain boundary decorated with MgZn<sub>2</sub>-particles

In alloy 1, large MgSnY-particles identified by STEM EDS were observed near grain boundaries and at sub-grain boundaries, in particular at the intersection of some lines of MgZn<sub>2</sub>-chains decorating sub-grain boundaries (Fig. 6).

Precipitation of an Mg<sub>2</sub>Sn-phase was clearly seen after aging for 1 day at 175 °C (Fig. 7). Plate-like Mg<sub>2</sub>Sn-particles were found coupled with MgZn<sub>2</sub>-needles inside the grain, as well as at sub-grain and grain boundaries.

Together with MgZn<sub>2</sub>-needles, they form T-shaped particles clearly seen at the sub-grain boundary (Fig. 7).

Zones depleted of precipitates near grain boundaries were observed even after 2 h of aging at 225 °C. Similar zones were found near sub-grain boundaries after 2 days of aging at 175–225 °C. Large particles inside these zones were identified by SEM/STEM EDS as MgSnY in alloy 1 and as Mg<sub>3</sub>Sb<sub>2</sub> in alloy 2. The subgrain microstructure, which makes itself evident by precipitate depleted zones, is clearly seen after long times of aging (Fig. 8). The width of the depleted zones increases with temperature and aging time. Outer borders of the depleted zones are adjoined by bands of enlarged precipitates having density smaller than that in the middle of sub-grains (Figs. 9, 10). As in earlier stages, the orientation of MgZn<sub>2</sub>-needles across a sub-grain boundary does not change.

#### Microhardness measurements

The mechanical properties of the alloys were examined using microhardness testing. The microhardness of the solution treated and aged Mg–Sn–Zn–Y and Mg–Sn–Zn–Sb alloys was measured for different aging times and temperatures (Fig. 11). For both alloys there are three distinctive peaks of microhardness in the aging curve.

Both alloys showed a substantial hardening effect up to 16 days of aging (Fig. 11). The alloy with Y addition exhibited better stability (increase in hardness of about 30% after 16 days of aging at 225 °C). The alloy with Sb addition showed structural stability during 12 days at 175 °C (25–30% hardening effect), but at 225 °C after 12 days of aging, the hardness exceeds the initial value by ~5% only (Fig. 11).

## Discussion

### Phase formation during solidification

Thermodynamic analysis of the quaternary systems Mg–Zn–Sn–Y and Mg–Zn–Sn–Sb performed with the ThermoCalc program (Fig. 12) shows that the formation temperatures of MgSnY and Mg<sub>3</sub>Sb<sub>2</sub> are different: the

**Fig. 6** TEM (a) and STEM (b) micrographs of Mg–Sn–Zn–Y alloy after aging for 16 h at 175 °C. Sub-grain boundaries (marked by arrows in (b)) decorated by chains of MgZn<sub>2</sub> particles between large MgSnY particles

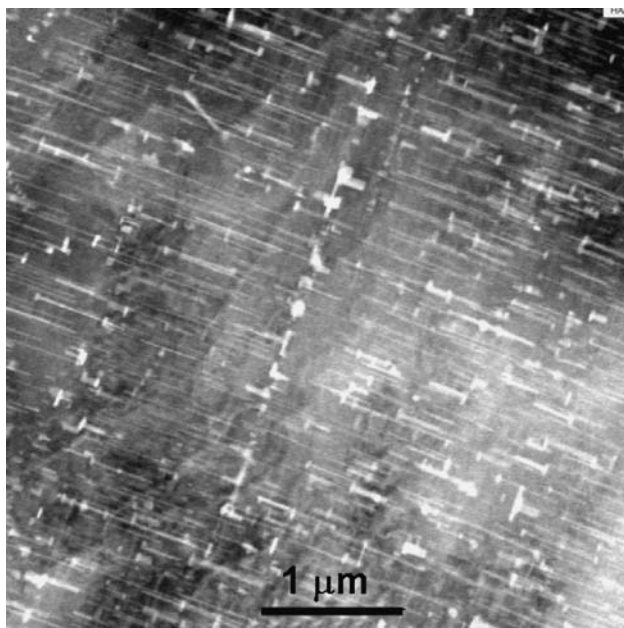
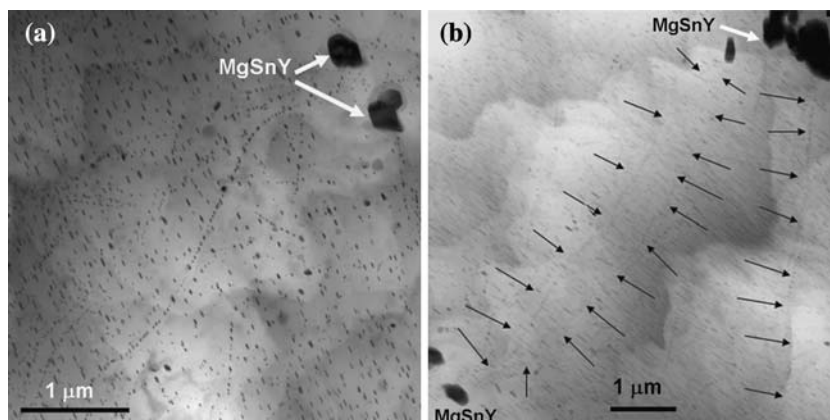
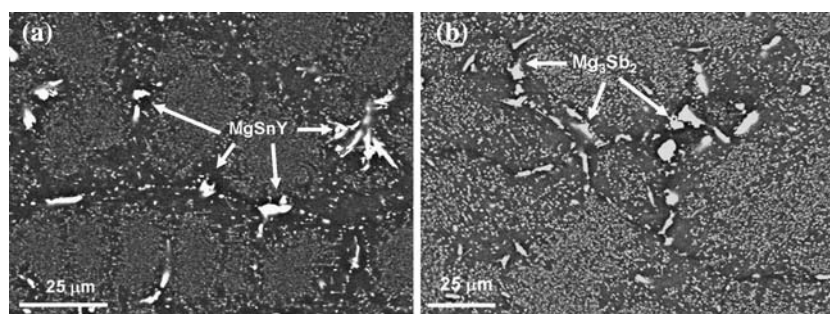


**Fig. 7** STEM micrograph of Mg–Sn–Zn–Y alloy after aging at 175 °C for 1 day. Two-phase particles consist of MgZn<sub>2</sub>-needles and Mg<sub>2</sub>Sn plate-like precipitates forming the T-shape particles

MgSnY phase starts to form at 570 °C (Fig. 12a) whereas the Mg<sub>3</sub>Sb<sub>2</sub> phase is formed below 525 °C (Fig. 12b). So MgSnY particles have more time to grow from the melt.

**Fig. 8** SEM micrographs of alloy 1 (a) and alloy 2 (b) after aging for 12 days at 225 °C; zones depleted of precipitates are formed near grain and sub-grain boundaries; large MgSnY (a) and Mg<sub>3</sub>Sb<sub>2</sub> (b) particles are located inside the depleted zones



Apparently this time was enough to consume all the dissolved Y, since no Y was detected in the α-Mg matrix. The volume fraction of MgSnY particles in alloy 1 is about 0.5%, and the one of Mg<sub>3</sub>Sb<sub>2</sub> particles in alloy 2 is about 0.3%.

It can be concluded that the additions of Y and Sb to the molten Mg lead to the formation of high temperature phases during solidification. In the case of Y this is the ternary phase MgSnY seen in Fig. 1b, and in the case of Sb, this is the binary phase Mg<sub>3</sub>Sb<sub>2</sub> seen in Fig. 1d.

As can be seen from microstructure study (Figs. 1, 9, 10) and from microhardness measurements (Fig. 11), the additions of Y and Sb cause a similar effect on the formation of sub-grain structure and aging behavior of the Mg–Sn–Zn alloy, however there is a quantitative difference between the two alloys. This difference originates from a difference in the size and shape of the HTP-particles. The average size of MgSnY particles is larger than that of Mg<sub>3</sub>Sb<sub>2</sub>. MgSnY particles grew up to 15 μm while Mg<sub>3</sub>Sb<sub>2</sub> particles did not grow over 5–7 μm. MgSnY particles look like elongated plates, whereas Mg<sub>3</sub>Sb<sub>2</sub> particles have a more rounded shape. These crystallized particles are concentrated in the last solidified regions between the dendrite arms. They did not dissolve during solution treatment at 440 °C as well as during exposure to elevated (aging) temperatures.

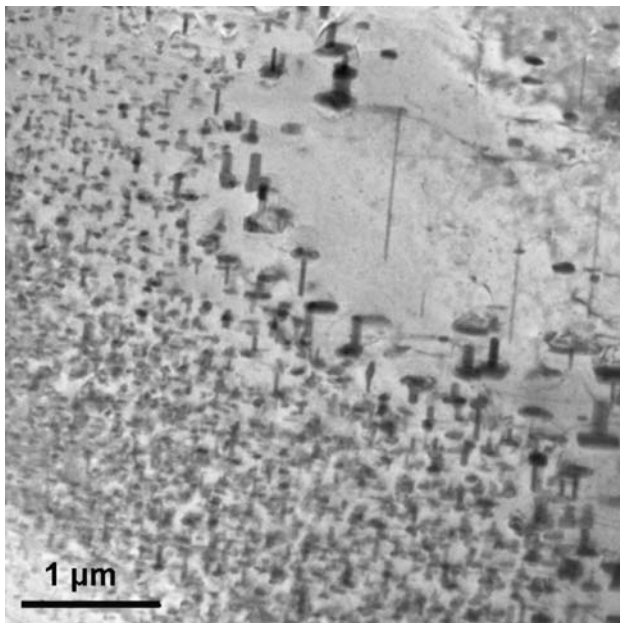


**Fig. 9** TEM micrograph of the MgSnZnSb specimen after aging for 4 days at 225 °C. Zone depleted of precipitates near the sub-grain boundary, adjoined by enlarged T-shaped precipitates with density smaller than that in the center of the sub-grain

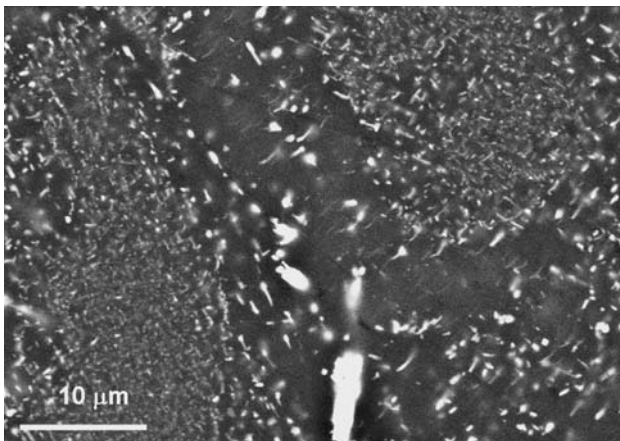


**Fig. 10** SEM micrograph of Mg–Sn–Zn–Y alloy after aging for 12 days at 225 °C

#### The influence of HTP-particles on the sub-grain microstructure formation

HTP-particles were located at grain- and sub-grain boundaries and sometimes at the intersections of sub-grain boundaries (Figs. 6, 8, 10), which is indicative of their influence on the microstructure formed. HTP-particles may serve as effective barriers for moving grain- and sub-grain boundaries, therefore restrain the growth and disappearance of sub-grains during solution treatment. As a result, a distinct sub-grain microstructure is preserved as opposed to

its absence in the base Mg–Zn–Sn alloy. These processes are schematically presented in Fig. 13.

Sub-grain boundaries are formed during solution treatment of the cast alloys. These low-angle boundaries are considered as plane dislocation arrays or dislocation walls [9]. These walls, if free from defects, can move and absorb each other (or annihilate with each other if they consist of opposite dislocations). Complete dissolution of the alloying elements (Zn and Sn) in the  $\alpha$ -Mg matrix during solution treatment makes the grain and sub-grain boundaries binary phase free. It may lead to the growth of sub-grains and to the annihilation of sub-grain boundaries during solution treatment, as was apparently the case with the base Mg–Zn–Sn alloy [1–3]. Small amount of undissolved HTP-particles (MgSnY or Mg<sub>3</sub>Sb<sub>2</sub> in our case) can restrain the recovery process during solution treatment [4, 5] and retain a fine sub-grain structure (Fig. 13b).

Precipitation of binary MgZn<sub>2</sub> and Mg<sub>2</sub>Sn phases at sub-grain boundaries during aging (Fig. 13c, e) makes them less mobile due to the pinning of dislocations forming these low grain boundaries. Such pinned sub-grain boundaries act as effective obstacles for plastic deformation. It manifests itself in the additional hardening comparing to the base alloy (Fig. 11), especially at long aging times.

#### Development of precipitate depleted zones

Increasing the aging time leads to the appearance of zones depleted of precipitates near grain- and sub-grain boundaries (Figs. 8–10). It is presented schematically in Fig. 13e. The formation of PD-zones is explained by near grain boundary (NGB) coarsening. The precipitates inside the grain are smaller than those at the boundary itself. It is connected with earlier nucleation of precipitates at grain boundaries and faster diffusion of the alloying elements along grain boundaries. Dissolution of precipitates in the NGB-zones is initially provided by diffusion from them to large precipitates at the grain boundary, and then also by diffusion from these smaller precipitates to the larger precipitates at the outer border of PD-zones. As a result, outer borders of the depleted zones are adjoined by bands of enlarged precipitates. These enlarged precipitates grow at the expense of smaller precipitates in the PD-zone, as well as smaller ones in the inner part of the adjacent sub-grain. As a result, they form a “crust” of the PD-zone (Figs. 9, 10, 13e). Being a diffusion controlled process, naturally the width of the depleted zones increases with temperature and aging time.

Such sub-grain boundaries, pinned by HTP-particles and by the coarsened binary MgZn<sub>2</sub> and Mg<sub>2</sub>Sn particles, enclosed by PD-zones with a “crust” of enlarged binary particles, are assumed to be an effective barrier for plastic deformation.

**Fig. 11** Microhardness of alloys 1 and 2 compared to the base Mg–Sn–Zn alloy [1]: (a) first 48 h of aging; (b) long times of aging

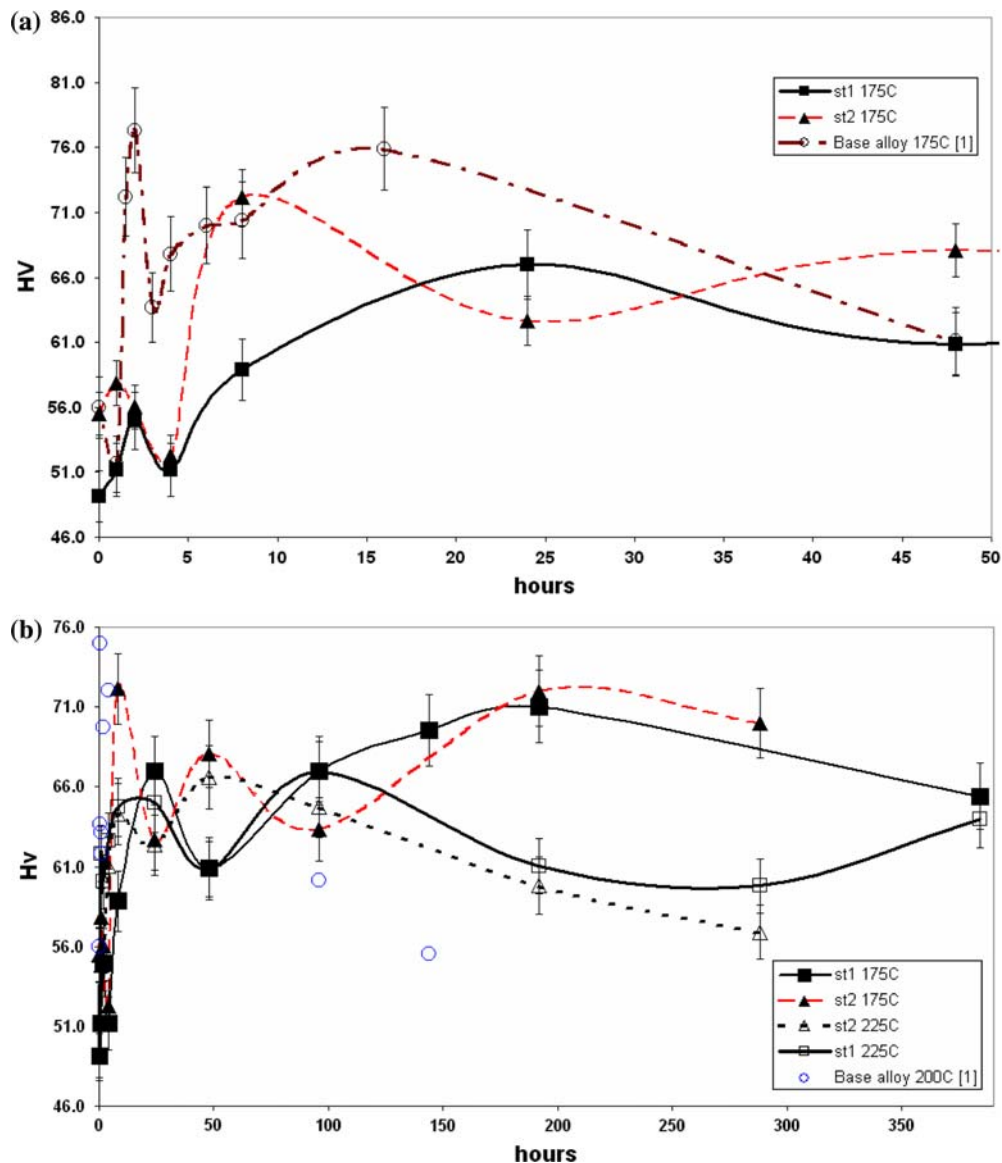
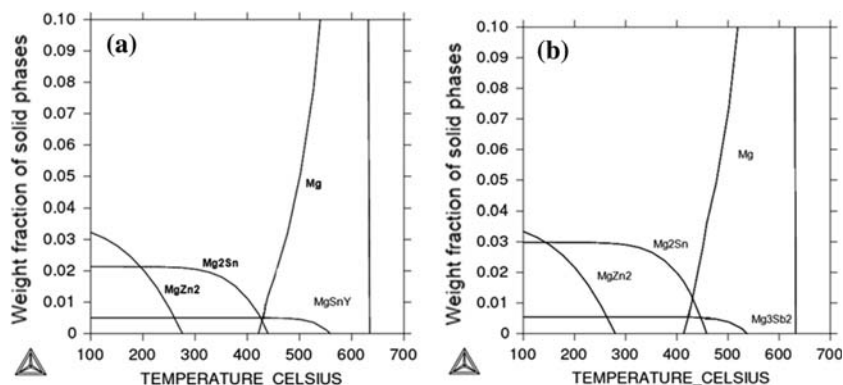


**Fig. 12** Phases at equilibrium as a function of the temperature: (a) Mg–Sn–Zn–Y alloy, (b) Mg–Sn–Zn–Sb alloy



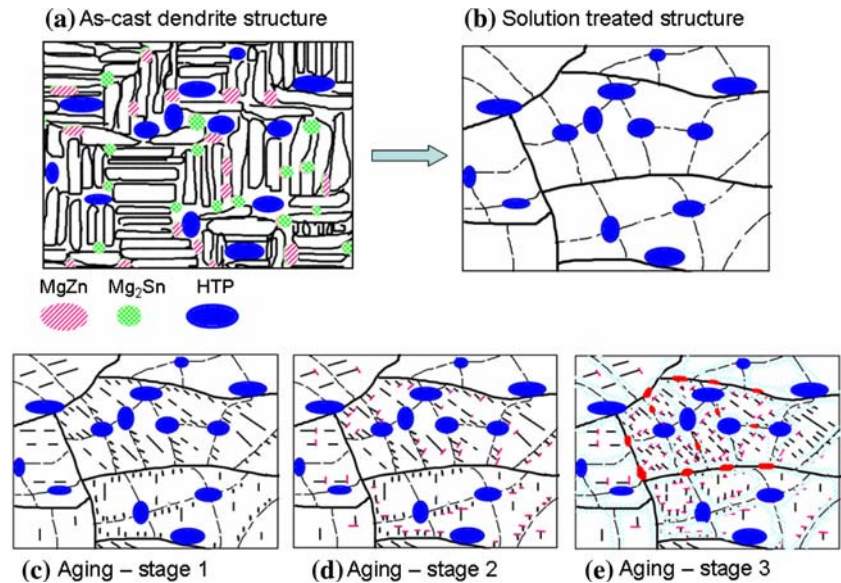
Precipitation hardening of alloys with additional sub-grain microstructure

The microhardness of solution treated specimens of the alloy with Y addition (~50 HV) and with Sb addition

(~55HV) [6] is similar to the one measured for the Mg–Zn–Sn base alloy (~56 HV) [1] (Fig. 11a).

Apparently, small amounts of HTP particles do not influence the dislocation movement, and therefore the hardness of solution treated alloys. Minor differences in

**Fig. 13** Microstructure evolution during casting (schematic) (a), solution treatment (b) and different stages of aging (c–e)



hardness are caused by different concentrations of alloying elements in the solid solution responsible for solution hardening.

The difference in hardness between the alloys with Sb and Y additions and the base alloy becomes apparent after ~48 h of aging at 175 °C (Fig. 11). At shorter times (less than 48 h), the hardness is determined by solid solution hardening and by precipitation of binary MgZn<sub>2</sub> and Mg<sub>2</sub>Sn particles in the bulk of grains. The base alloy had a slightly higher Sn concentration (4.7% wt.) and Zn concentration (4.5% wt.) than that of the Mg–Sn–Zn–Y and Mg–Sn–Zn–Sb investigated alloys (see Table 1). Therefore, the first two hardness peaks in the base alloy are higher than the corresponding peaks in alloys 1, 2 (Fig. 11a). As previously found [1, 2], the first peak is connected with the precipitation of MgZn<sub>2</sub> (it corresponds to stage 1 of aging, (Figs. 53 and 13c) and the second one to the formation of the Mg<sub>2</sub>Sn phase (stage 2, Figs. 7 and 13d). The latter process is controlled by bulk diffusion of Sn and corresponds to a hardness peak in the binary Mg–Sn–alloy [4].

On the other hand, alloys 1 and 2 exhibited a substantial hardening effect of up to 16 days of aging whereas the base alloy underwent overaging after 4 days at 200 °C (Fig. 11b). This difference is apparently caused by the presence of an additional sub-grain microstructure in the alloys with Y and Sb additions. The HTP MgSnY- and Mg<sub>3</sub>Sb<sub>2</sub>-particles formed during casting appeared to be effective barriers for moving sub-grain boundaries during solution treatment. By this way, they preserved an additional sub-grain microstructure. Sub-grain boundaries serve as additional places for heterogeneous nucleation of precipitates during aging. The curved chains of MgZn<sub>2</sub>-needles (Figs. 5, 6) revealed the existence of sub-grain boundaries. Following the

heterogeneous nucleation of Mg<sub>2</sub>Sn and the formation of chains of T-shaped particles along a sub-grain boundary, the latter became almost immobile.

At longer times, the alloys with Y and Sb additions showed the third peak of hardness (Fig. 11b). This peak can be attributed to further strengthening of the sub-grain structure caused by the formation of depletion zones and a “crust” of enlarged particles near grain- and sub-grain boundaries (stage 3, Fig. 13e). The formation of depletion zones adjoined by the “crust” of enlarged T-shaped particles (Figs. 9, 10) completes the boundary pinning. Such fixed sub-grain boundaries may serve as a strong barrier for moving dislocations thereby strengthening the alloy.

In fact, the aged stabilized sub-grain structure corresponds to a decrease in the effective average grain size (from ~50–80 μm to ~20–30 μm) that can be attributed to an increase of ~30% in microhardness (Fig. 11). It is responsible for the observed structural stability of the alloys at elevated temperatures.

## Conclusion

Structural stability of the Mg–Zn–Sn alloy at elevated temperatures was substantially improved by small additions of Y and Sb. High temperature phases, MgSnY and Mg<sub>3</sub>Sb<sub>2</sub>, were formed in the as-cast alloys.

They remained unchanged during solution treatment at 440 °C and aging at 175–225 °C. These HTP-particles were concentrated in the interdendritic areas and then, after solution treatment, at sub-grain and grain boundaries. These particles pinned the sub-grain boundaries preventing a sub-grain growth during heat treatment. As a result, an additional sub-grain microstructure, in comparison with the



base Mg–Zn–Sn alloy, remained in the Mg–Zn–Sn–Y and Mg–Zn–Sn–Sb alloys after solution treatment.

Precipitation hardening of these alloys occurred in three stages. At the first stage, MgZn<sub>2</sub>-needles precipitated homogeneously inside the grains, as well as at grain- and sub-grain boundaries. At the second stage of aging, the Mg<sub>2</sub>Sn-phase precipitated heterogeneously, mainly at the MgZn<sub>2</sub>-needles. The formation of T-shaped particles along grain- and sub-grain boundaries stabilized the microstructure and improved the mechanical properties by decreasing the effective grain size. The third stage is connected with the formation of depleted zones near grain- and sub-grain boundaries enclosed by “crusts” of enlarged T-shaped particles. Such pinned sub-grain microstructure appeared to be moderately stable at elevated temperatures.

**Acknowledgements** The study was partially supported by the Fund for the Promotion of Research at the Technion. The foundation is acknowledged for its support.

## References

1. Cohen S, Goren-Muginstein GR, Abraham S, Dehm G, Bamberger M (2003) Phase formation, precipitation and strengthening mechanisms in Mg–Zn–Sn and Mg–Zn–Sn–Ca alloys. In: Proceedings of the TMS annual meeting, San Diego, CA, 2 March 2003, p. 301
2. Cohen S, Goren-Muginstein GR, Abraham S, Rashkova B, Dehm G, Bamberger M (2005) *Z Metallkd* 96:1081
3. Rashkova B, Keckes J, Levi G, Gorny A, Bamberger M, Dehm G (2006) Microstructure Evolution and Phase Formation in Novel Mg–Zn-Based Alloys, Magnesium. In: Kainer KU (ed) Proceedings of the 7th International conference on magnesium alloys and their applications. DGM, Dresden, Germany, 6–9 November 2006, p 486
4. Sasaki TT, Oh-ishi K, Ohkubo T, Hono K (2006) *Scripta Materialia* 55:251
5. Mendis CL, Bettles CJ, Gibson MA, Hutchinson CR (2006) *Mater Sci Engineer* A435–436:163
6. Guangyin Y, Yangshan S, Wenjiang D (2000) *Scripta Mater* 43:1009
7. Guangyin Y, Yangshan S, Wenjiang D (2001) *Mater Sci Engineer* A308:38
8. Gorny A, Goren-Muginstein GR, Katsman A, Dehm G, Rashkova B, Bamberger M (2006) The influence of Y additions on precipitation sequence in Mg–Zn–Sn based alloy. In: Proceedings of the TMS annual meeting, San Antonio, Texas, USA, 12–16 March 2006, pp 387
9. Porter DA, Easterling KE (2004) Phase transformations in metals and alloys. CRC Press, Taylor&Francis Group, Boca Raton, FL, p 514